Time-resolved dose reconstruction by motion encoding of volumetric modulated arc therapy fields delivered with and without dynamic multi-leaf collimator tracking

THOMAS RAVKILDE[1,2], PAUL J. KEALL[3], CAI GRAU[1,2], MORTEN HØYER[1,2] & PER R. POULSEN[1,2]

[1]*Department of Oncology, Aarhus University Hospital, Aarhus, Denmark,* [2]*Institute of Clinical Medicine, Aarhus University, Aarhus, Denmark, and* [3]*Radiation Physics Laboratory, University of Sydney, Sydney, Australia*

Corresponding author: T. Ravkilde, Department of Medical Physics, Aarhus University Hospital, Nr. Brogade 44, 8000 Aarhus C, Denmark. E-mail: thomas. ravkilde@rm.dk.

Abstract

Background. Organ motion during treatment delivery in radiotherapy (RT) may lead to deterioration of the planned dose, but can be mitigated by dynamic multi-leaf collimator (DMLC) tracking. The purpose of this study was to implement and experimentally validate a method for time-resolved motion including dose reconstruction for volumetric modulated arc therapy (VMAT) treatments delivered with and without DMLC tracking.

Material and methods. Tracking experiments were carried out on a linear accelerator (Trilogy, Varian) with a prototype DMLC tracking system. A motion stage carrying a biplanar dosimeter phantom (Delta4PT, Scandidos) reproduced eight representative clinical tumor trajectories (four lung, four prostate). For each trajectory, two single-arc 6 MV VMAT treatments with low and high modulation were delivered to the moving phantom with and without DMLC tracking. An existing in-house developed program that adds target motion to treatment plans was extended with the ability to split an arc plan into any number of sub-arcs, allowing the calculated dose for different parts of the treatment to be examined individually. For each VMAT sub-arc, reconstructed and measured doses were compared using dose differences and 3%/3 mm γ-tests.
Results. For VMAT sub-arcs the reconstructed dose distributions had a mean root-mean-square (rms) dose difference of 2.1% and mean γ failure rate of 2.0% when compared with the measured doses. For final accumulated doses the mean rms dose difference was 1.6% and the γ failure rate was 0.7%.

Conclusion. The time-resolved motion including dose reconstruction was experimentally validated for complex tracking and non-tracking treatments with patient-measured tumor motion trajectories. The reconstructed dose will be of high value for evaluation of treatment plan robustness facing organ motion and adaptive RT.

Introduction

In radiotherapy (RT), organ motion during treatment delivery may lead to deterioration of the planned dose distribution [1,2]. A promising method to account for the intrafraction motion is dynamic multi-leaf collimator (DMLC) tracking where the planned MLC aperture is continuously adapted to the real-time monitored target position [3–6]. Motion including dose reconstruction is possible for tumor tracking since the required knowledge of intrafraction target motion is readily available. One avenue towards motion including dose reconstruction is the utilization of a clinical treatment planning system (TPS). This approach allows use of institutionally validated dose calculation algorithms and evaluation of the reconstructed dose in the clinical environment.

Several methods have been proposed to estimate the impact of rigid tumor motion with a commercial TPS by convolving the probability density function (PDF) of the target position with either the static three-dimensional (3D) dose distribution [7,8] or the incident two-dimensional (2D) photon fluence of each treatment beam [9–11]. However, convolution methods cannot account for interplay effects in dynamic RT treatments where MLC motion takes place during beam-on periods. An alternative method is to model target motion by isocenter shifts [12,13]. In a previous paper, a simple and automatic method that models target motion by splitting the original treatment fields into a multitude of sub-beams with different isocenter shifts was presented [14].

In this study we refine this method with temporal resolution by allowing reconstruction of the target dose distribution at several time points throughout delivery of a VMAT field to a moving target and validate it experimentally for complex treatments.

Material and methods

Experiments

Electromagnetic (EM)-based DMLC tracking experiments were carried out on a Trilogy linear accelerator equipped with a 120 leaf Millennium MLC (Varian Medical Systems, CA, USA) and a prototype DMLC tracking system [4]. A schematic representation of the experiment setup is provided in Supplementary Figure 1. During experiments, a Delta4PT phantom (Scandidos, Sweden) [15] with two orthogonal planar diode arrays (total of 1069 diodes) encased in cylindrical PMMA measured the delivered time-resolved dose distribution at a rate of 72 Hz. Routine clinical calibration of the Delta4PT phantom was performed prior to measurements.

As described in the Supplementary Appendix, a programmable motion stage [16] was modified to carry the phantom on a platform made of wood. The motion stage reproduced eight patient-measured tumor trajectories representing different motion patterns; four lung trajectories ("Typical" motion, High- frequency breathing, Predominantly left-right motion, and Baseline shifts) and four prostate trajectories (Continuous drift, Persistent excursion, Transient excursion, and High-frequency excursions). A detailed explanation of the tumor trajectories and their selection can be found in Keall et al. [17]. For each trajectory, two 358° single arc 6 MV RapidArc VMAT plans with low and high modulation were delivered to the moving phantom. Details of the VMAT plans have been published previously [17,18]. The VMAT treatments were delivered for each trajectory with and without DMLC tracking, as well as to a static phantom for reference.

The 3D target position was measured at 30 Hz by an EM transponder system (RayPilot, Micropos Medical, Sweden). During tracking the position was transmitted to the tracking software for continuous adaptation of the MLC aperture. For lung tumor trajectories, prediction was used to compensate for the tracking system latency, which was previously measured to be 140 ms [19]. Tracking log files with the gantry angle and real-time measured target position and Dynalog files [20] with the MLC positions, gantry angle, and beam-on flag were stored for each experiment along with the time-resolved Delta4PT phantom measurements.

Dose reconstruction and comparison with measurements

The data flow is illustrated in Supplementary Figure 2. The dose delivered in each treatment was reconstructed and compared with the measured dose distribution. The dose reconstruction was made with a previously published method that mimics target motion as isocenter shifts [14], and which was expanded for this study to allow dose reconstruction for any division of a VMAT field into sub-arcs. In the current study, the 358° VMAT fields were divided into 10 sub-arcs of 35.8°, resulting in a relatively coarse time resolution with the reconstructed dose distribution determined for each individual tenth of the VMAT treatments. First, the Dynalog files of each experiment were synchronized to the tracking log files (and thereby the phantom motion) by use of the gantry angle. Next, an in-house developed computer program (written in Matlab, MathWorks Inc., MA, USA) was used to generate a motion mimicking Dicom treatment plan with the actual MLC positions recorded in the Dynalog files and a multitude of sub-beams with isocenter shifts that corresponded to the real-time recorded target positions. Unlike Poulsen et al. [14], the Dynalog recorded MLC positions were used in the dose reconstruction not only for tracking, but also for non-tracking treatments. A bin width of 1 mm was used, i.e. all measured target positions within a 1 mm^3 cube were given the same isocenter shift. Each motion mimicking Dicom plan had approximately 1500 control points.

The motion mimicking treatment plan was imported into the treatment planning system (Eclipse 10.0.28, Varian Medical Systems), where the motion including dose distribution was calculated using the Anisotropic Analytical Algorithm (AAA) and subsequently exported as a 3D dose matrix for each sub- beam in a grid with voxels of 2.5 mm sides. Next, a second in-house developed Matlab program added all sub-beam dose matrices belonging to each VMAT sub-arc, thus creating the 3D dose distribution delivered during each sub-arc (i.e. during each tenth of the VMAT field).

In order to compare the reconstructed doses with the measurements, the dose at the discrete positions of the Delta4PT phantom diodes was extracted from the reconstructed 3D dose distributions correcting for small spatial offsets caused by slight off-isocenter positioning of the phantom. For temporal synchronization of measured and reconstructed doses, the phantom data were synchronized with the treatment delivery by means of the beam-on flag in the Dynalog files. Measured doses were then accumulated for each VMAT sub-arc producing 10 doses to compare with the reconstructed doses. At posterior gantry angles the entrance beam passed through the couch, the EM antennae system, and the platform carrying the phantom. The damping of these objects was measured as a function of gantry angle for the central diode in the phantom and used as a common gantry dependent correction factor for the measured dose for each diode.

The reconstructed dose distributions were com- pared with the diode measurements for each sub-arc, and for the accumulated dose of the complete arc field, by means of the dose difference and a γ-test [21] with the 3%/3 mm pass criteria used for daily quality assurance (QA) in our clinic. The root-mean- square (rms) dose difference was determined in percentage of the maximum measured dose for the sub-arc (or complete arc field). The γ value was calculated for each diode using the 2D distance to agreement in the diode planes. Diodes with accumulated measured doses below 5% of the maximum accumulated dose in the measured static reference were excluded in the calculations of both dose differences and γ-tests. Statistical significance analysis of differences in rms dose differences and γ failure rates for sets of experiments used a two-sample Student's t-test with a 5% significance level.

In the interest of investigating the ability of the dose reconstruction to predict the impact of a given target motion on a given VMAT plan, the γ failure rate of the reconstructed dose delivered to a *moving* phantom using the reconstructed *static* phantom dose as reference was calculated and compared with the same γ failure rate calculation based on the measured doses.

Results

Figure 1 illustrates the impact of motion on the dose distribution for a selected experiment. Comparison of the left and middle columns qualitatively shows that for non-tracking treatment delivery to the moving phantom, the dose became smeared out and a systematic shift of the dose in the caudal direction (down in Figure 1) occurred in both individual VMAT sub-arcs and the accumulated dose of the complete arc fields. Redistribution of dose due to interplay effects was also seen in some sub-arcs. Tracking to a large extent restored the moving phantom dose distribution to that of a static phantom (right column). A single diode in the Delta4PT phantom was non-functioning. As this diode invariably measured zero dose, it was automatically excluded from calculations of dose differences and γ-tests due to the < 5% dose exclusion criterion.

The time-resolved doses for three sample diodes in Figure 2 show that phantom motion had a large effect on the doses near high dose gradients (green) for non-tracking treatments, but that this effect was largely reduced by tracking. However, motion only marginally disturbed the dose in low dose gradient regions (red, blue) for both tracking and non-tracking experiments. For all three sample diodes the time- resolved reconstructed dose was in good agreement with the measurements (mean rms difference of 0.7% averaged over all VMAT sub-arcs).

Averaging over all experiments and all included diodes, doses were reconstructed with a mean rms dose difference relative to the experiments of 2.1% for VMAT sub-arcs and of 1.6% for doses accumulated over the complete arc fields. Table I presents the rms dose difference for each individual VMAT plan. The mean rms dose difference was significantly higher for high modulation VMAT plans than for low modulation plans ($p < 0.001$ for both sub-arcs and the complete arc fields). The mean rms dose difference was also higher for the investigated lung plans than for the prostate plans for both individual VMAT sub-arcs ($p < 0.001$) and doses accumulated over the complete arc fields ($p = 0.040$). The rms dose difference for doses to a moving phantom compared to a static phantom was not statistically significant ($p=0.92$ for sub-arcs and $p=0.96$ for complete arc fields).

The mean γ failure rate was 1.6% for doses of VMAT sub-arcs and 0.7% for accumulated doses of the complete arc fields. Table II lists γ failure rates of the reconstructed dose for each individual VMAT plan. The γ failure rates were significantly higher for reconstructed doses of high modulation plans than of low modulation plans accumulated over the complete arc fields ($p = 0.005$) but not for sub-arcs ($p = 0.32$). The γ failure rates were significantly higher for reconstructed doses of lung VMAT plans than of prostate VMAT plans ($p < 0.001$) for both VMAT sub-arcs and the complete arc fields.

As shown in Figure 3 the reconstructed motion induced γ failure rates in the delivered target dose distributions (using static doses as reference) in general agreed well with the corresponding γ failure rates in the measured doses. The rms deviation between measured and reconstructed γ failure rates was 1.5%.

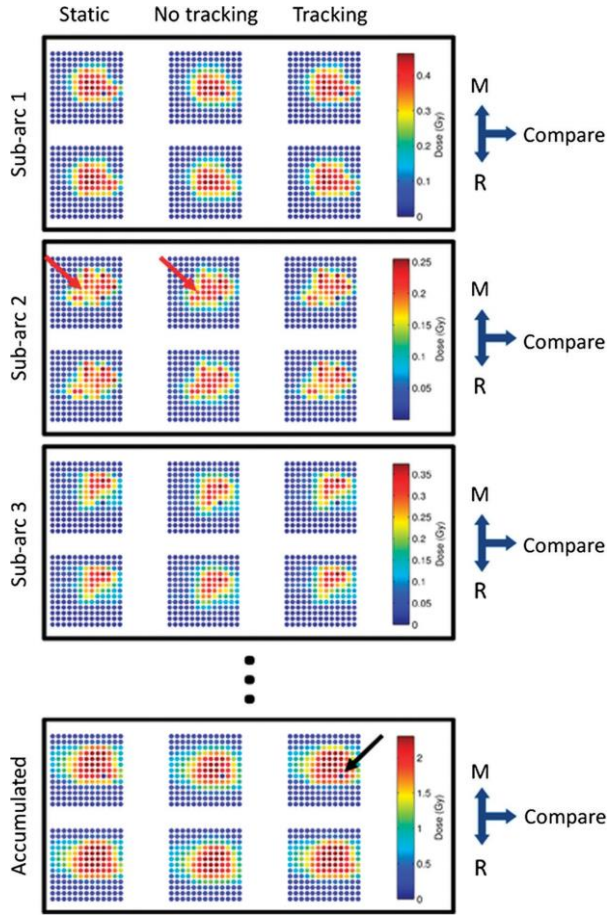

Figure 1. A representative example of measured (M) and reconstructed (R) doses for the high modulation volumetric modulated arc therapy (VMAT) lung plan delivered with the high frequency lung motion trajectory. The dose in the central 6 X 6 cm of one of the biplanar arrays is displayed for the first three VMAT sub-arcs (i.e. first three tenths of the VMAT field) as well as accumulated for the entire VMAT field. The three columns show the dose of a static phantom (left), a moving phantom without tracking (middle), and a moving phantom with tracking (right). One diode was broken (marked with a black arrow) and invariably showed zero in the measured dose.The red arrow marks an example of dose redistribution due to interplay effects in this specific VMAT sub-arc.

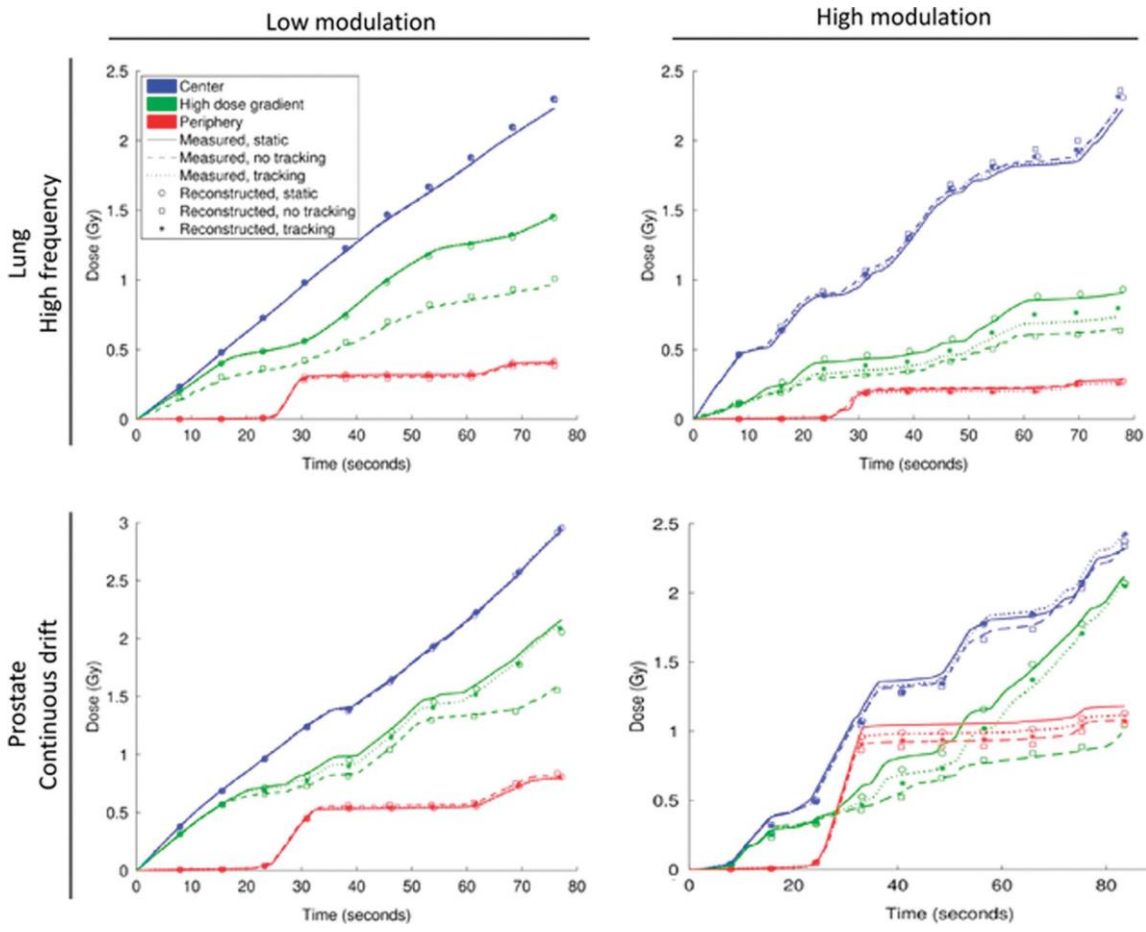

Figure 2. Measured (curves) and reconstructed (symbols) cumulative doses in three sample diodes in the Delta4PT phantom: the diode in the center of the phantom (blue), a diode in a high dose gradient (green), and a diode in the periphery of the phantom (red). Doses are shown for the static phantom (full line) as well as the moving phantom without (dashed line) and with (dotted line) tracking. Top: high and low modulation lung VMAT plans with the high frequency lung tumor motion trajectory. Bottom: high and low modulation prostate VMAT plans with the Continuous drift prostate motion trajectory. The central and peripheral diodes were the same for all plots, whereas the high dose gradient diode differed between lung and prostate VMAT plans.

Table I. Results of dose reconstruction quantified by dose differences to the measured dose.

Plan	Static	Motion, no tracking	Motion, tracking	All
Dose for VMAT sub-arcs				
Lung, low modulation	2.5%	2.3 [2.0,2.6]%	2.3 [2.2,2.5]%	2.4 [2.0,2.6]%
Lung, high modulation	2.6%	2.8 [2.4,3.2]%	2.5 [2.3,2.7]%	2.7 [2.3,3.2]%
Prostate, low modulation	1.5%	1.6 [1.5,1.7]%	1.6 [1.5,1.9]%	1.6 [1.5,1.9]%
Prostate, high modulation	1.7%	1.9 [1.7,2.0]%	1.8 [1.7,2.0]%	1.8 [1.7,2.0]%
Accumulated dose for complete arc field				
Lung, low modulation	1.9%	1.7 [1.5,2.0]%	1.7 [1.5,1.8]%	1.7 [1.5,2.0]%
Lung, high modulation	2.1%	2.2 [1.9,2.3]%	2.0 [2.0,2.1]%	2.1 [1.9,2.3]%
Prostate, low modulation	0.8%	0.8 [0.8,0.9]%	0.8 [0.7,0.9]%	0.8 [0.7,0.9]%
Prostate, high modulation	1.6%	1.8 [1.7,2.0]%	1.9 [1.7,2.1]%	1.8 [1.6,2.1]%

Mean [and range] of root-mean-square dose differences between measured and reconstructed dose distributions in percentage of the maximum measured dose, averaged over the four trajectories investigated for each plan. Results are shown both for the dose delivered in each VMAT sub-arc (i.e. each tenth of the VMAT field, top four rows) and for the complete arc field (bottom four rows).

Discussion

A method for time-resolved dose reconstruction of moving targets by means of motion mimicking Dicom treatment plans was demonstrated and experimentally validated in two orthogonal planes for complex rotational RT treatments with and with- out DMLC tracking. The method provided similar agreement between reconstructed and measured doses for deliveries to static and moving phantoms with and without tracking, indicating that the motion encoded dose reconstruction is on par with that of the well-established and commonly applied method for daily QA using the Delta4PT phantom. This accuracy is also available with temporal resolution, which enables pinpointing of temporal errors in treatment delivery [22]. The dose reconstruction was found to be more challenged by plans with high modulation than with low modulation. Even so, the highest mean rms difference between reconstructed and measured dose distributions was 3.2% (high modulation lung plan, "Typical" trajectory, averaged over 10 VMAT sub-arcs).

In this study the dose reconstruction was also found to be more challenging for the investigated lung treatments than for prostate treatments, but the cause is not obvious. The difference could be due to the faster and larger magnitude of lung tumor motions or the considerable difference in target volume between the lung and prostate treatment plans. Other indirect causes for the difference are also possible, such as difference in plan complexity due to different OAR being included in the inverse optimization.

The mean γ failure rates of accumulated reconstructed doses (0.7% with 3%/3 mm pass criteria) are slightly higher than those found previously for DMLC tracking of conformal fields (0.5% with 2%/2 mm pass criteria) [14], which is to be expected due to the higher plan complexity. Other groups have recalculated doses delivered with VMAT using the actual leaf motions from Dynalog files with comparable results [23,24], but these studies do not include motion effects or offer temporal resolution. To the best of our knowledge, only one previous study provides reconstruction of temporally resolved motion-affected doses [25]. In that study the original treatment plan was morphed based on measured data and then perturbed with rigid motion to achieve γ failure rates of 90.6–95% (3%/3 mm criteria) for reconstructed doses of moving phantoms.

In the present study the entirety of the treatment delivery was split into 10 sub-arcs providing relatively coarse temporal resolution, but the method could in principle be used to split an RT arc treatment plan into any number of smaller sub-arcs. However, the higher temporal resolution comes at the expense of speed and the complications of managing large amounts of data. Ideally, the dose reconstruction method should be fast enough to allow dose reconstruction and dose error estimations in real time. The present dose reconstruction method is also limited by treating tissue motion as rigid translations, ignoring tissue deformations [26–28]. No trajectories were available for healthy tissues. Doses to OAR, which often do not move rigidly with the tumor [29], were therefore considered outside the scope of the present study. The motion of healthy tissues may also affect the dose to the tumor, but such variations are not accounted for in the current study. Although the thorax is highly inhomogeneous, both lung and prostate plans were measured and reconstructed using a homogeneous phantom. Doing so is, however, in accordance with common QA procedure [15,30].

The TPS-based dose reconstruction allows for application of other dose calculation algorithms as well [14,31,32] and enables calculation of standard clinical measures of dose coverage, such as dose- volume histograms. The method presented here is therefore widely applicable for interfractional adaptive RT, where knowledge of dose to a moving target, accumulated over a single or several fractions, could be of value.

In summary, the time-resolved motion including dose reconstruction was experimentally validated for complex tracking and non-tracking treatments. The reconstructed dose will be of high value for evaluation of treatment plan robustness facing organ motion and adaptive RT.

Table II. Results of dose reconstruction quantified by γ-tests using measured dose as reference.

Plan	Static	Motion, no tracking	Motion, tracking	All
Mean γ failure rates for VMAT sub-arcs				
Lung, low modulation	4.60%	3.4 [2.8,3.9]%	3.6 [3.3,4.5]%	3.6 [2.8,4.6]%
Lung, high modulation	2.60%	3.1 [2.4,3.6]%	1.8 [1.5,2.2]%	2.5 [1.5,3.6]%
Prostate, low modulation	0.60%	0.7 [0.5,0.9]%	0.8 [0.5,1.1]%	0.8 [0.5,1.5]%
Prostate, high modulation	0.90%	1.5 [1.3,2.0]%	1.1 [0.9,1.4]%	1.1 [0.8,2.0]%
γ failure rates for complete arc field				
Lung, low modulation	1.30%	0.5 [0.3,0.8]%	0.8 [0.3,1.0]%	0.7 [0.3,1.3]%
Lung, high modulation	2.30%	2.3 [1.4,2.7]%	1.5 [0.9,2.1]%	2.1 [0.9,2.7]%
Prostate, low modulation	0.00%	0.0 [0.0,0.0]%	0.0 [0.0,0.0]%	0.0 [0.0,0.0]%
Prostate, high modulation	0.10%	0.1 [0.0,0.6]%	0.1 [0.0,0.3]	0.1 [0.0,0.6]%

Mean [and range] of 3%/3 mm γ failure rates of reconstructed dose distributions compared with measurements, averaged over the four trajectories investigated for each plan. Results are shown averaged over the ten individual VMAT sub-arcs (top four rows) and for the complete arc field (bottom four rows).

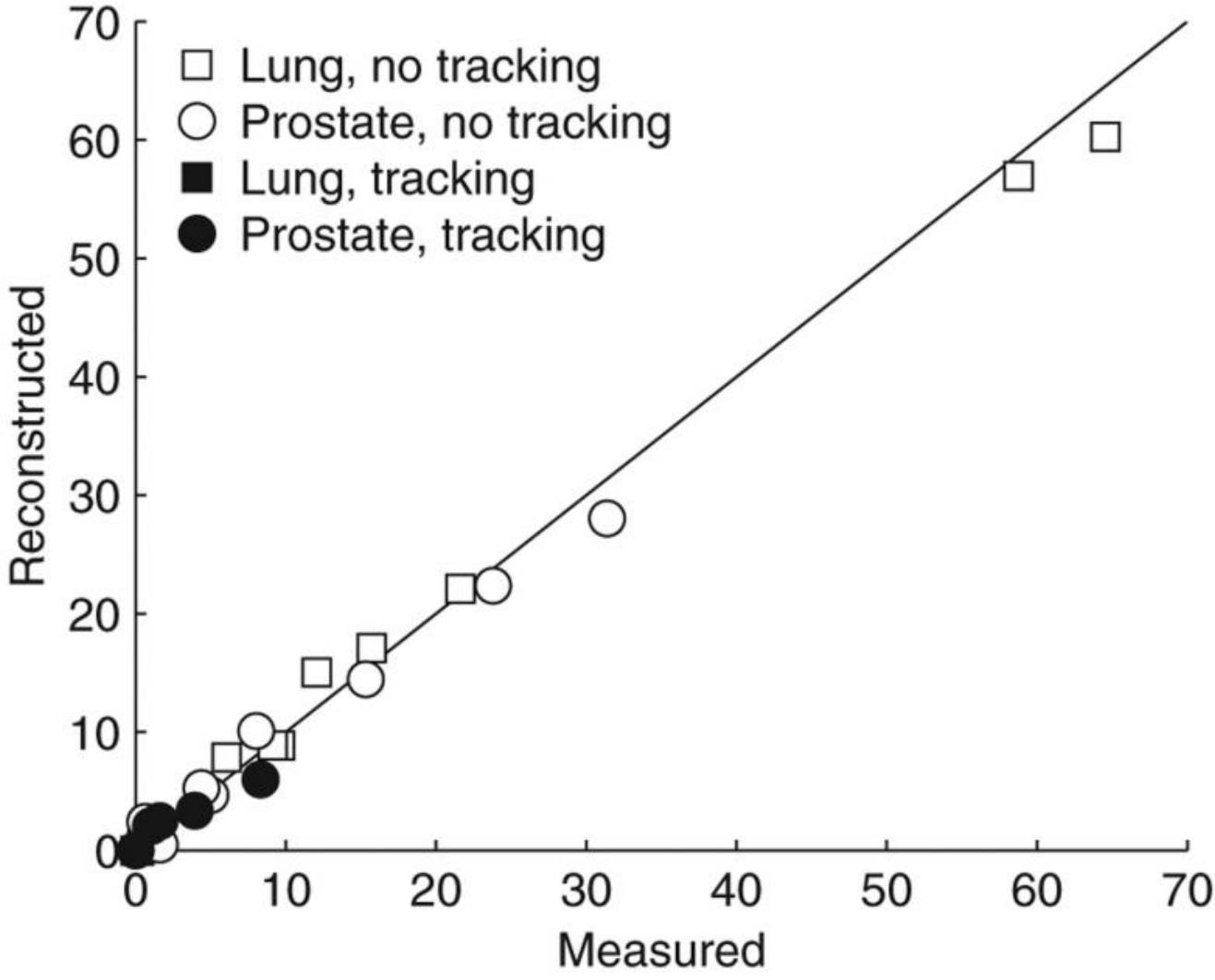

Figure 3. 3%/3 mm γ failure rates in the final accumulated dose delivered to the moving target with (closed symbols) and without (open symbols) dynamic MLC tracking for lung (squares) and prostate (circles) VMAT plans. The reference dose for the γ-test was the dose to the static phantom. The scatter plot compares the γ failure rate in the measured doses with the γ failure rate in the reconstructed doses for the 32 combinations of VMAT treatment plans, motion trajectories, and tracking or no tracking. The line of unity is shown in black.

Acknowledgements

We gratefully thank Drs Patrick Kupelian (University of California, Los Angeles) and Katja Langen (MD Anderson Cancer Center, Orlando) for the prostate trajectories, Drs Yelin Suh (MD Anderson Cancer Center) and Sonja Dieterich (University of Califor- nia, Davis) for the lung tumor trajectories, Görgen Nilsson and Peter Münger (Scandidos) for modifications of the Delta4PT software to allow export of time-resolved dose data, and Roman Iustin and Andreas Bergqvist (Micropos Medical AB) for modifications of the RayPilot system to allow integration with the tracking program.

Declaration of interest: The authors report no conflicts of interest. The authors alone are responsible for the content and writing of the paper.

This work was supported by NCI Grant R01CA93626 and by The Danish Cancer Society, CIRRO (The Lundbeck Foundation Center for Interventional Research in Radiation Oncology), The Danish Council for Strategic Research, and Varian Medical Systems. Aarhus University Hospital, Denmark, received financial support through a research agreement with Varian Medical Systems, Palo Alto, CA.

References

[1] Keall PJ, Mageras GS, Balter JM, Emery RS, Forster KM, Jiang SB, et al. The management of respiratory motion in radiation oncology report of AAPM Task Group 76. Med Phys 2006;33:3874.

[2] Depuydt T, Poels K, Verellen D, Engels B, Collen C, Haverbeke C, et al. Initial assessment of tumor tracking with a gimbaled linac system in clinical circumstances: A patient simulation study. Radiother Oncol 2013;106:236–40.

[3] McQuaid D, Webb S. IMRT delivery to a moving target by dynamic MLC tracking: Delivery for targets moving in two dimensions in the beam's eye view. Phys Med Biol 2006;51: 4819–39.

[4] Sawant A, Venkat R, Srivastava V, Carlson D, Povzner S, Cattell H, et al. Management of three-dimensional intrafraction motion through real-time DMLC tracking. Med Phys 2008;35:2050–61.

[5] Krauss A, Nill S, Tacke M, Oelfke U. Electromagnetic real-time tumor position monitoring and dynamic multileaf collimator tracking using a Siemens 160 MLC: Geometric and dosimetric accuracy of an integrated system. Int J Radiat Oncol Biol Phys 2011;79:579–87.

[6] Crijns SPM, Raaymakers BW, Lagendijk JJW. Proof of concept of MRI-guided tracked radiation delivery: Tracking one-dimensional motion. Phys Med Biol 2012;57:7863.

[7] Lujan AE, Larsen EW, Balter JM, Haken RKT. A method for incorporating organ motion due to breathing into 3D dose calculations. Med Phys 1999;26:715–20.

[8] Liu Y, Shi C, Lin B, Ha CS, Papanikolaou N. Delivery of four-dimensional radiotherapy with TrackBeam for moving target using an AccuKnife dual-layer MLC: Dynamic phantoms study. J Appl Clin Med Phys 2009;10:2926.

[9] Chetty IJ, Rosu M, Tyagi N, Marsh LH, McShan DL, Balter JM, et al. A fluence convolution method to account for respiratory motion in three-dimensional dose calculations of the liver: A Monte Carlo study. Med Phys 2003;30:1776–80.

[10] Langen KM, Chauhan B, Siebers JV, Moore J, Kupelian PA. The dosimetric effect of intrafraction prostate motion on step-and-shoot intensity-modulated radiation therapy plans: Magnitude, correlation with motion parameters, and comparison with helical tomotherapy plans. Int J Radiat Oncol Biol Phys 2012;84:1220–5.

[11] Aristophanous M, Rottmann J, Court LE, Berbeco RI. EPID-guided 3D dose verification of lung SBRT. Med Phys 2011;38:495–503.

[12] Naqvi SA, D'SouzaWD. A stochastic convolution/superposition method with isocenter sampling to evaluate intrafraction motion effects in IMRT. Med Phys 2005;32:1156–63.

[13] Berbeco RI, Hacker F, Zatwarnicki C, Park S-J, Ionascu D, O'Farrell D, et al. A novel method for estimating SBRT delivered dose with beam's-eye-view images. Med Phys 2008;35:3225–31.

[14] Poulsen PR, Schmidt ML, Keall P, Worm ES, Fledelius W, Hoffmann L. A method of dose reconstruction for moving targets compatible with dynamic treatments. Med Phys 2012; 39:6237–46.

[15] Bedford JL, Lee YK, Wai P, South CP, Warrington AP. Evaluation of the Delta^4 phantom for IMRT and VMAT verification. Phys Med Biol 2009;54:N167–76.

[16] Malinowski K, Noel C, Lu W, Lechleiter K, Hubenschmidt J, Low D, et al. Development of the 4D Phantom for patient- specific, end-to-end radiation therapy QA. In: Proceedings of SPIE. San Diego, CA, USA; 2007. p. 65100E–65100E–9.

[17] Keall PJ, Sawant A, Cho B, Ruan D, Wu J, Poulsen P, et al. Electromagnetic-guided dynamic multileaf collimator tracking enables motion management for intensity-modulated arc therapy. Int J Radiat Oncol Biol Phys 2011;79:312–20.

[18] Poulsen PR, Fledelius W, Cho B, Keall P. Image-based dynamic multileaf collimator tracking of moving targets during intensity-modulated arc therapy. Int J Radiat Oncol Biol Phys 2012;83:e265–71.

[19] Ravkilde T, Keall PJ, Højbjerre K, Fledelius W, Worm E, Poulsen PR. Geometric accuracy of dynamic MLC tracking with an implantable wired electromagnetic transponder. Acta Oncol 2011;50:944–51.

[20] Litzenberg DW, Moran JM, Fraass BA. Verification of dynamic and segmental IMRT delivery by dynamic log file analysis. J Appl Clin Med Phys 2002;3:63–72.

[21] Low DA, Harms WB, Mutic S, Purdy JA. A technique for the quantitative evaluation of dose distributions. Med Phys 1998;25:656.

[22] RavkildeT, Keall PJ, Grau C, Høyer M, Poulsen PR. PD-0342 Time-resolved evolvement of target dose distributions during IMAT with and without dynamic MLC tracking. Radiother Oncol 2012;103:S137.

[23] Teke T, Bergman AM, Kwa W, Gill B, Duzenli C, Popescu IA. Monte Carlo based, patient-specific RapidArc QA using Linac log files. Med Phys 2010;37:116–23.

[24] Schreibmann E, Dhabaan A, Elder E, Fox T. Patient-specific quality assurance method for VMAT treatment delivery. Med Phys 2009;36:4530–5.

[25] Feygelman V, Stambaugh C, Zhang G, Hunt D, Opp D, Wolf TK, et al. Motion as a perturbation: Measurement- guided dose estimates to moving patient voxels during modulated arc deliveries. Med Phys 2013;40:021708.

[26] Sharma M, Weiss E, Siebers JV. Dose deformation- invariance in adaptive prostate radiation therapy: Implica- tion for treatment simulations. Radiother Oncol 2012; 105:207–13.

[27] Li XA, Liu F, Tai A, Ahunbay E, Chen G, Kelly T, et al. Development of an online adaptive solution to account for inter- and intra-fractional variations. Radiother Oncol 2011; 100:370–4.

[28] Nyeng TB, Kallehauge JF, Høyer M, Petersen JBB, Poulsen PR, Muren LP. Clinical validation of a 4D-CT based method for lung ventilation measurement in phantoms and patients. Acta Oncol 2011;50:897–907.

[29] Thörnqvist S, Bentzen L, Petersen JBB, Hysing LB, Muren LP. Plan robustness of simultaneous integrated boost radiotherapy of prostate and lymph nodes for different image-guidance and delivery techniques. Acta Oncol 2011; 50:926–34.

[30] Falk M, af Rosenschöld PM, Keall P, Cattell H, Cho BC, Poulsen P, et al. Real-time dynamic MLC tracking for inversely optimized arc radiotherapy. Radiother Oncol 2010; 94:218–23.

[31] Fogliata A, Scorsetti M, Navarria P, Catalano M, Clivio A, Cozzi L, et al. Dosimetric comparison between VMAT with different dose calculation algorithms and protons for soft-tissue sarcoma radiotherapy. Acta Oncol 2013;52: 545–52.

[32] Hoffmann L, Jørgensen M-BK, Muren LP, Petersen JBB. Clinical validation of the Acuros XB photon dose calculation algorithm, a grid-based Boltzmann equation solver. Acta Oncol 2012;51:376–85.